Cost Comparison for Different PV-Battery System Architectures Including Power Converter Reliability

Cost Comparison for Different PV-Battery System Architectures Including Power Converter Reliability

Martijn Deckers[1,*,**], Leander Van Cappellen[*,***], Glenn Emmers[*,**], Fereshteh Poormohammadi[*,**], and Johan Driesen[*,**]

[*]EnergyVille - Thor Park 8301, 3600 Genk, Belgium
[**]ESAT/ELECTA KU Leuven - Kasteelpark Arenberg 10, 3001 Heverlee, Belgium
[***]IMO-IMOMEC Hasselt University - Wetenschapspark 1, 3590 Diepenbeek, Belgium
[1]martijn.deckers@kuleuven.be

Acknowledgments

This work has been supported by Flanders Innovation & Entrepreneurship and Flux50 under project DAPPER, HBC.2020.2144. Martijn Deckers is funded by a PhD grant of the Research Foundation Flanders (FWO), 1S87522N.

Keywords

≪Levelized cost of energy≫, ≪Renewable energy systems≫, ≪Reliability≫, ≪Aging≫, ≪Batteries≫.

Abstract

This paper compares the levelized energy cost of a commercial DC-coupled photovoltaic battery systems with a multiple input multiple output converter. The comparison is based on an electrothermal simulation allowing to include the actual converter efficiency and degradation in different use cases. The multiple input multiple output converter proofs to be less expensive and more reliable, however, the lower efficiency causes the final levelized energy cost to be higher.

Introduction

Currently, two categories of residential photovoltaic (PV) battery systems are commercially available, AC- and DC-coupled systems. The AC-coupled systems are mostly applied in a retrofit installation when the addition of a battery is wanted to an already operational PV system. This corresponds to the system in Fig. 1 a), the PV panels are connected to the AC grid using a DC/DC converter followed by a DC/AC converter and the battery has its own DC/DC and DC/AC converter in parallel, both of which need to be bidirectional to allow for either charging and discharging of the battery. The DC-coupled systems allows to eliminate one of the DC/AC converters by connecting the DC/DC converters to a common DC bus as shown in Fig. 1 b). Next to the use of less components, generally the efficiency improves as two conversion steps are eliminated when excess PV power is transferred to the battery [1]. Next to these two commercial system architectures, also a third topology is emerging. Here the number of converter modules is reduced further by combining two DC/DC converters into one Multiple Input Multiple Output (MIMO) converter as shown in Fig. 1 c). This decreases the number of components and conversion steps even further [2]. A good measure to compare these different systems architectures is the Levelized Cost Of Energy (LCOE) which reflects the cost of a kWh of energy consumed taking into account all the expenses and gains during the lifetime of the system [3].

The paper is organised as follows. First, the gaps in current literature are identified followed by the objectives of this work. Secondly, the method used to calculate the LCOE is elaborated starting from

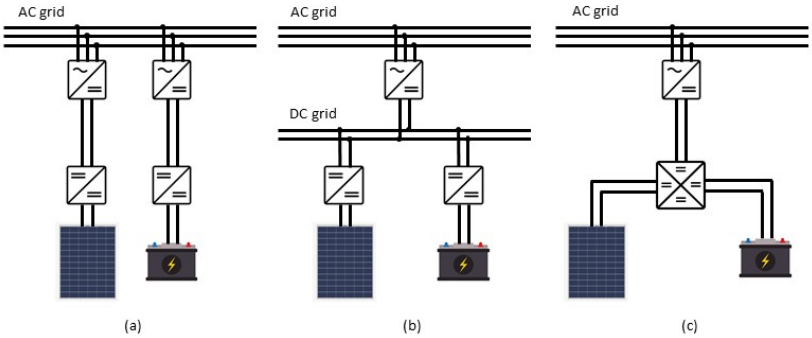

Fig. 1: System structure of (a) an AC coupled system, (b) a DC-coupled system and (c) a MIMO converter.

the main LCOE formula after which the individual terms such as cost, efficiency and reliability are discussed. Thirdly, the used converter architectures and their parameters are given. Fourthly, the results are presented after which the paper is summarised in the final section.

Scope of the paper

Reliability comparisons between commercial DC- and AC-coupled topologies can be found in literature [4]. To the authors knowledge these analyses do not yet exist for the newer MIMO topologies. These new systems could have great potential but more work is needed to quantify this. Also the LCOE analysis of a standard PV battery systems can be found in literature. To determine the power flow based on given mission profiles, mostly ideal battery dispatching is used which will also be done in this paper. However, frequently some additional simplifications are made which might have a big impact on the final results [3, 5, 6]. Summarised the following gaps are identified in the existing research:

- Currently no LCOE evaluation is available for MIMO converters in PV-battery systems;
- The efficiency is treated as a fixed value instead of being a function of the power flow;
- The component degradation is not taken into account or a fixed lifetime is assumed.

This paper aims to compare the LCOE of a commercial DC-coupled system with a MIMO architecture as presented in Fig. 1 b) and c). This LCOE will take into account the system construction costs, the operational efficiency and component degradation, potentially causing the need for system maintenance or replacement. The differences in LCOE between the two configurations will be highlighted together with the main causes for these discrepancies. A sensitivity analysis towards the cost, efficiency, lifetime and converter specifications will take into account modelling uncertainties and show how future changes might influence the result.

Levelized cost of energy (LCOE) calculation method

This section describes the method used for the LCOE calculation. After elaborating the base formula, also the individual terms such as manufacturing cost, reliability and efficiency will be discussed.

Base formula

The LCOE evaluates the costs and revenues generated with the setup during its operational lifetime, taking into account a certain discount rate r. Equation 1 gives the main expression for the LCOE, it is calculated in a similar way as shown in [7] with a few changes to allow the inclusion of variable efficiencies and degradation.

$$LCOE = \frac{C_{PV} + C_{inverter} + C_{E\ purchased} - C_{E\ sold}}{E_{load}} \tag{1}$$

The cost of the inverter system $C_{inverter}$ is the main scope of the paper. The different architectures use different components, leading to a different manufacturing cost $C_{inverter\ manufacturing}$ and the degradation

during its lifetime may differ, leading to discrepancies in operation and maintenance cost $C_{inverter\ o\&m}$ as given in equation 2. The cost of the purchased energy $C_{E\ purchased}$ and the sold energy $C_{E\ sold}$ can be set depending on different scenarios. The battery is always dispatched in the most economic way satisfying the required load energy E_{load}. The cost of the PV panels C_{PV} will not be the focus of this paper as it is the same for all the different system architectures.

$$C_{inverter} = C_{inverter\ manufacturing} + \sum_{n=0}^{N} \frac{C_{inverter\ o\&m}}{(1+r)^n} \tag{2}$$

$$C_E = \sum_{n=0}^{N} \frac{C_{E\ n}}{(1+r)^n} \tag{3}$$

An important aspect in this paper is that the conversion efficiencies $\eta_{storage->out}$, $\eta_{PV->storage}$ and $\eta_{PV->out}$ will not be taken constant but instead are a function of the actual energy-flows based on the electrothermal simulation.

$$E_{load} = E_{out} + E_{purchased} - E_{sold} \tag{4}$$

$$E_{out} = \sum_{n=0}^{N} (E_{out\ load} + E_{out\ sold}) = \sum_{n=0}^{N} (\eta_{PV->out}\ E_{PV\ out} + \eta_{storage->out}\ E_{storage\ out}) \tag{5}$$

$$\sum_{n=0}^{N} E_{PV} = \sum_{n=0}^{N} (E_{PV\ out} + E_{PV\ storage}) \tag{6}$$

$$\sum_{n=0}^{N} E_{storage\ in} = \sum_{n=0}^{N} (\eta_{PV->storage}\ E_{PV\ storage}) \tag{7}$$

Summarised, LCOE differences between system architectures can be caused by: 1) Differences in initial investment due to the dependence on the number of components and needed component ratings. 2) The power flow dependent conversion efficiencies between PV panels, battery and output energy which are dependent on the number of conversion steps. 3) Differences in system reliability which are dependent on the component ratings and the component stress.

Converter manufacturing cost

The manufacturing costs $C_{DCcoupled}$ and C_{MIMO} of the two converter architectures need to be estimated. For this a base cost C_{base} is calculated, taking the switching devices, diodes, inductors, heat sinks and cooling fans costs $C_{Component\ n}$ into account. The used cost values are based on the single unit price of a component n with the correct rating. In Fig. 2 an example is shown from the search for heat sinks and their price in function of the thermal resistance. Other components such as capacitors, PCB, casing, etc. are excepted to be similar for both architectures and can be modelled as an additional cost $C_{additional}$ which is the same for both architectures. At this point, additional parameters such as labour, transportation, engineering, etc. are not taken into account. To acquire a realistic price estimate for both systems, the current market price C_{market} for a DC-coupled PV systems with similar ratings is chosen as the cost $C_{DCcoupled}$ in this analysis. The cost of the MIMO converter C_{MIMO} is then calculated based on C_{market} and the relative difference between the estimated base costs C_{base} of the two converters ΔC keeping the ratio constant.

$$C_{base} = \sum_{n=0}^{N} C_{Component\ n} + C_{additional} \tag{8}$$

$$\Delta C[-] = \frac{C_{base\ MIMO}}{C_{base\ DCcoupled}} - 1 \tag{9}$$

$$C_{DCcoupled} = C_{market} \tag{10}$$

$$C_{MIMO} = C_{market}(1 + \Delta C) \tag{11}$$

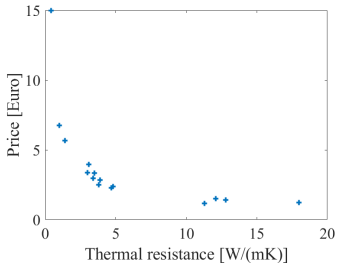

Fig. 2: The cost of a heat sink in function of the required thermal resistance.

Converter efficiency and degradation modelling

Electrothermal simulation

The electrothermal simulation is done based on an electrical and a thermal model. For the electrical model, a set of equations is written based on the schematics in Fig. 4, relating the voltages and currents. For the MIMO converter multiple sets of equations are used for each operational condition. Different sets of equations are used for both the continuous and discontinuous operation modes of the converters. The thermal model uses a lumped network of thermal resistances which can be found in the component data-sheets. Thermal capacitances will not be considered, meaning that the system is always in steady state. The coupling between thermal and electrical simulation is done using a temperature dependent drain to source resistance $R_{DS\,on}$. An iteration between the electrical and thermal model results in a lookup table relating the converter power to the component die temperatures and losses. This allows to convert the mission profile into temperature profiles and to calculate the efficiency.

Degradation modelling

For the degradation modelling, the main focus is placed on the switching devices. The failure rates of the capacitors improved drastically with the use of film capacitors. When the switch is operated within specifications, package failures caused by thermal stress contribute most to the degradation. The main failure modes are bondwire degradation and die solder layer delamination. To calculate the amount of damage a certain temperature cycle invokes, an empirical model is used. The number of cycles is counted using the rainflow counting algorithm. When the failure criteria are met, components need to be replaced leading to increased operation and management costs in the LCOE [4, 8, 9]. Here the assumption is made that when a component fails, the entire power electronic system is replaced. A frequently used thermal degradation model is the Bayerer model given in Equation 12. Here the number of cycles in a lifetime N_f is linked to the junction temperature swing ΔT_j, the minimum junction temperature $T_{j\,min}$ and the heating time t_{on}. Additionally, the bondwire configuration is taken into account by including the bond wire current I and the thickness of the bondwire D. The device voltage class V estimates the device thickness [10, 11]. Often a set of default fitting parameters is used called the CIP08 model [13] which is used in this paper as well. This model was developed for standard Si power modules while the components used in this paper are SiC components. Even when the failure modes are very similar, care should be taken when this lifetime model is applied to different technologies as proven in [12]. Because of this, the lifetime results will be normalised for comparison and a base lifetime of 15 year will be used in the LCOE calculations. This means the DC-coupled system gets a default lifetime of 15 years and the lifetime model will determine the difference that needs to be added or subtracted to get the MIMO converter lifetime.

$$N_f = A\ (\Delta T_j)^{\beta_1}\ e^{\frac{\beta_2}{T_{jmin}+273}}\ t_{on}^{\beta_3}\ I^{\beta_4}\ V^{\beta_5}\ D^{\beta_6} \tag{12}$$

The total workflow is shown in Fig. 3. In step one the temperature profile of each component is obtained based on the lookup tables and the power flows determined by the converter control. Applying rainflow counting to this temperature profile and using the reliability model, the expected time of failure is obtained in step two. A Monte Carlo analysis can be used to take into account uncertainties and translate

this one point in time into a failure probability distribution. In step three the integral is taken to get the unreliability function. This function can easily be converted to the reliability function. Integrated, this gives the Mean Time To Failure (MTTF) which is used to estimate the maintenance costs.

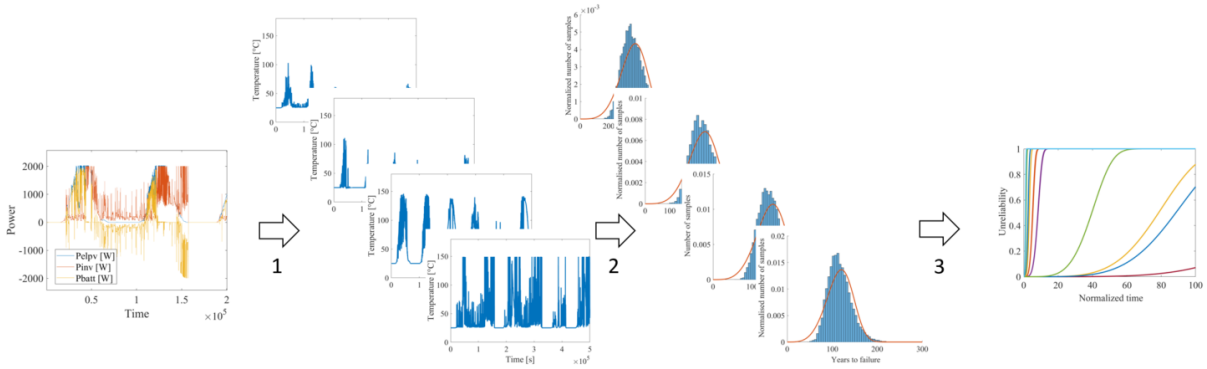

Fig. 3: Workflow to calculate the unreliability of the different switching devices based on a mission profile.

Converter design, specifications and control

In this section the converter system architectures are described in more detail. The used specifications and control methodology will be given as well.

Converter topologies

In Fig. 4 the converter schematics used in the simulation are given. The circuits are selected to be the most basic topologies achieving the required functionality such as the ability to have a bidirectional power flow to the battery. The PV converter is a basic boost converter and the battery converter is a synchronous boost converter [4]. The MIMO converter is synthesised from the combination of boost converters to achieve the same capabilities making this the simplest MIMO converter that can achieve the required functionality [14].

Converter specifications and control

The converter specifications used are summarised in the Table I. The power limits and voltages are the same for both the DC-coupled and MIMO converter. The inductances are converter specific as the DC-coupled requires two inductors while the MIMO converter only has one. The inductors values are chosen to ensure a similar current ripple for both the DC-coupled and MIMO converter.

In this work a policy case with different injection and consumption tariffs is implemented. As a result, the used control aims to maximise self consumption. This means that the produced PV power is used to satisfy the load and excess energy is transferred to the battery. When PV production is smaller than the load, energy from the battery is used to supply the difference. Within this control scheme, the limits of the different power converters in the system are also taken into account, possibly leading to curtailment

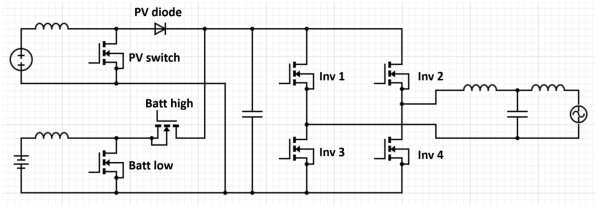

(a) Schematic of the DC-coupled converter

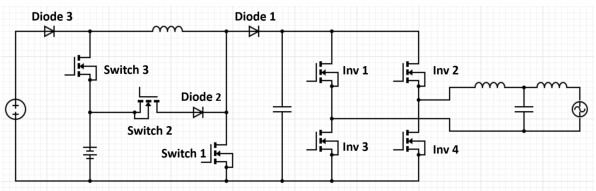

(b) Schematic of the MIMO converter

Fig. 4: Converter schematics used in the simulation.

of the PV by deviating from MPP and limiting the power transferred from or to the battery. The battery also has limited energy storage capacity. When the battery is full, excess PV energy will be sold to the grid and when it is empty, energy will be bought from the grid if needed. Fig. 5 shows a section form the load profile, electrical PV energy and the battery state of charge. The curtailment of the PV production can be seen as well as the maximum and minimum battery state of charge.

Table I: General converter specifications and converter components.

Parameter	Symbol	Value	Unit
General converter parameters			
Maximum PV power	Ppv_{max}	2000	W
Maximum PV voltage	Vpv_{max}	350	V
minimum PV voltage	Vpv_{min}	40	V
Battery voltage	$Vbatt$	350	V
Battery charging power	$Pbatt_{max}$	2000	W
Battery discharging power	$Pbatt_{min}$	-2000	W
Battery energy content	$Qbatt$	6000	Wh
Inverter maximum power	$Pinv_{max}$	2000	W
DC bus voltage	$Vbus$	450	V
Grid RMS voltage	$Vgrid$	230	Vrms
Grid frequency	$fgrid$	50	Hz
Switching frequency	fs	100000	HZ
DC-coupled converter parameters			
PV converter inductance	Lpv	0.0024	H
Battery converter inductance	$Lbatt$	0.0027	H
MIMO converter parameters			
MIMO inductance	L	0.0015	H
Used components			
SiC mosfet	IMW65R107M1H		
SiC diode	AIDW40S65C5		
PV panel	UL-305M-60		

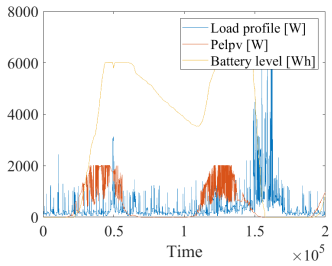

Fig. 5: Battery state of charge based on the load profile and the PV energy production.

In order to get a realistic power flow, real load and irradiance data are needed. For this work second resolution load data from HTW Berlin University of Applied Sciences [15] and second resolution irradiance data from the University of New South Wales [16] was used.

Results and discussion

In this section the simulation results are discussed. First the lifetime, converter manufacturing cost and efficiency are treated after which the final LCOE is calculated using these parameters. At the end a small sensitivity analysis on the LCOE will be conducted to examine the effects of potential modelling errors in the simulation.

The comparison of a DC-coupled and MIMO converter has been conducted for two main design cases. In the first case, the size of the heat sink is determined by the component that dissipated the most heat. Based on the maximum allowable die temperature the required heat sink was calculated and the same sink was then given to all the components. Because of this, the thermal cycling amplitudes are different for all components and the lifetime is mostly determined by the amount of dissipation rather than the number of cycles. In the second case, the required heat sink was calculated for each component independently, leading to smaller heat sink sizes for the non-restrictive components. This means that all components have similar thermal swings and the lifetime will be determined by the amount of cycles it undergoes.

Converter manufacturing cost

The manufacturing converter cost is evaluated for both the case with identical heat sinks and the case with optimised heat sinks. The used simulation values as well as the thermal resistances of the heat sinks in the optimised case can be found in Table II. The cost of the heat sinks are determined based on Fig 2. The diode and switch costs are equal for all devices because of the very similar required maximum ratings.

The MIMO converter appears to be the least expensive option as can be seen in Fig. 6. The cost of the DC-coupled converter with optimised sinks is set to 1. The main contributor to the cost is the inductor of which the MIMO only needs one. The MIMO converter has more components and a bit more losses leading to larger heat sinks expenses. Notwithstanding, the overall analyses remains in the advantage of the MIMO converter.

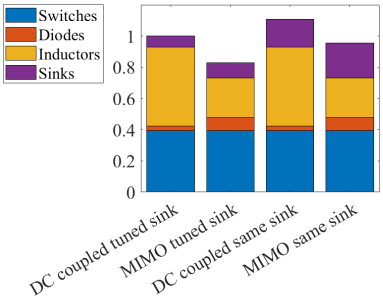

Fig. 6: Normalised cost of the DC-coupled and MIMO converter.

Table II: Optimised heat sink values and cost estimation parameters.

DC-coupled		**MIMO**		**Simulation parameters**	
Component	Thermal resistance	Component	Thermal resistance	Parameter	Value
Batt low	36.8000 W/(mK)	Switch 1	3.2600 W/(mK)	C_{base}	800 Euro
Batt high	20.5800 W/(mK)	Switch 2	7.9900 W/(mK)	$C_{E\ offtake}$	20 c/kWh
PV switch	3.2500 W/(mK)	Switch 3	20.9000 W/(mK)	$C_{E\ injection}$	-16 c/kWh
PV diode	23.8400 W/(mK)	Diode 1	23.8600 W/(mK)	r	0.05 [-]
Inv 1-4	23.1900 W/(mK)	Diode 2	18.4000 W/(mK)	C_{switch}	10 Euro
		Diode 3	6.9200 W/(mK)	C_{diode}	5 Euro
		Inv 1-4	23.1900 W/(mK)		

Lifetime

The resulting unreliability curves from the identical sink case can be seen in Fig. 7a and 7b. The MTTF of all the components are also summarised in Table III. The MTTF of the DC-coupled topology is normalised to 1. From this it can be seen that the MIMO topology is most reliable. The main restricting components are PV switch and switch 1. PV switch handles the PV power flow while switch 1 handles both the PV power flow and battery discharging. The reason for this higher reliability of switch 1 is the smaller boost ratios between the PV and battery voltage while in the DC-coupled converter everything

has to be boosted to the DC bus voltage. The same analysis is also done with an infinite battery size. The reliability of the inverter components decreases as well as those involved in charging and discharging the battery.

Fig. 7c and 7d give the reliability curves for the case with optimised sinks. Now the lifetime will no longer be determined by the temperature swing amplitudes but rather by the number of cycles. The inverter switches are the most limiting for the lifetime which is to be expected as they are operational when either PV energy goes to the load or the battery discharges. The second most lifetime restricting components are batt low and switch 3. This shows that the battery discharging causes a lot af thermal cycles. Switch 3 is more reliable because it does not have to switch when the battery keeps discharging between switching periods lowering the amount of thermal cycles. PV switch and switch 1 now have very high MTTF because their low reliability was purely caused by the large thermal cycle amplitude compared to the other components.

The same lifetime model is applied to the diodes giving an idea of their contribution to the system failure. Because of the high losses caused by the forward voltage they are susceptible to large temperature swings and can be limiting for the lifetime as well. The model was not made for these types of components but the similar packaging allows to make a first estimate.

Table III: MTTF of DC-coupled and MIMO converter components while using identical and optimised heat sinks.

Same sink				**Optimised sink**			
DC-coupled		**MIMO**		**DC-coupled**		**MIMO**	
Component	MTTF	Component	MTTF	Component	MTTF	Component	MTTF
Tot	1	Tot	2.08	Tot	1	Tot	1.01
Batt low	455.20	Switch 1	2.08	Batt low	2.52	Switch 1	159.74
Batt high	94.62	Switch 2	32.26	Batt high	5.10	Switch 2	87.56
PV switch	1.00	Switch 3	119.71	PV switch	77.66	Switch 3	5.23
PV diode	436.03	Diode 1	142.39	PV diode	8.24	Diode 1	3.20
Inv 1-4	58.51	Diode 2	121.81	Inv 1-4	1.37	Diode 2	8.14
		Diode 3	10.84			Diode 3	39.18
		Inv 1-4	58.51			Inv 1-4	1.37

Efficiency

The efficiency difference is compared in Fig. 8. The MIMO converter experiences less inductor loss as well as less losses in the switches as a result of the reduced voltage ratios. The forward voltages of the diodes cause a large loss increase resulting in a slightly lower average efficiency for the MIMO converter.

LCOE

Finally the resulting LCOE for the optimised sink case is shown in Fig. 9. It is clear that the converter efficiency is very important because of the large amount of energy that is processed by the installation during its lifetime. The additional cost of installing the system on location is not taken into account so the real LCOE will be higher, however, the relative difference remains the same. Table IV shows the final results achieved. Although the MIMO converter has a lower manufacturing cost and higher reliability, the slightly lower efficiency leads to a higher LCOE. The influence of the inverter is excluded in the MTTF of the optimised sink case to focus the results on the differences in the system.

In Fig. 10 a sensitivity analysis is included on the impact of the relative difference in cost, efficiency and MTTF. The current estimate is indicated with a dashed line. The parameters of the DC-coupled system are kept constant while the parameters of the MIMO converter are varied. The influence of the MTTF shows discrete steps as a prolonged lifetime might make it possible to buy one unit less during the system lifetime. At the end the inverter cost saturates as only one unit is purchased in the beginning.

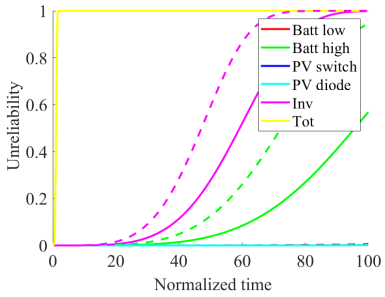

(a) Unreliability of the DC-coupled system with finite (full line) and infinite battery (dashed line). All the heat sinks have the same size.

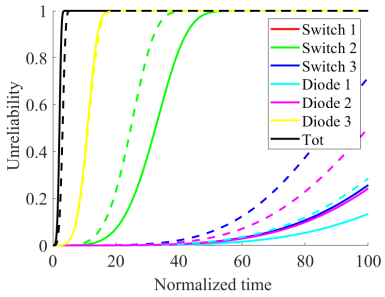

(b) Unreliability of the MIMO system with finite (full line) and infinite battery (dashed line). All the heat sinks have the same size.

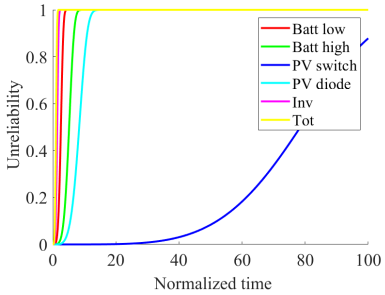

(c) Unreliability of the DC-coupled system where all the heat sinks are optimised to the same maximum temperature.

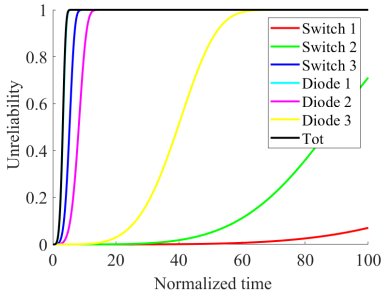

(d) Unreliability of the MIMO system where all the heat sinks are optimised to the same maximum temperature.

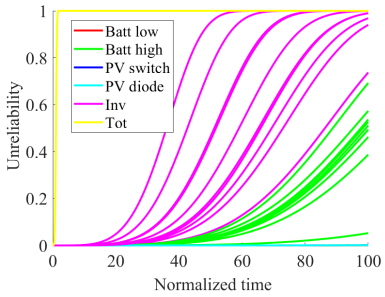

(e) Unreliability of the DC-coupled system for different load profiles. All the heat sinks have the same size.

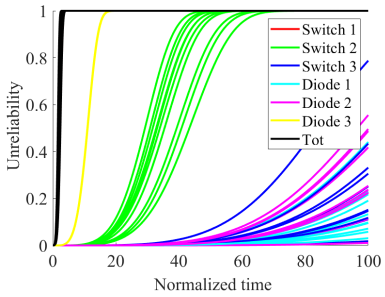

(f) Unreliability of the MIMO system for different load profiles. All the heat sinks have the same size.

Fig. 7: Results of the lifetime study.

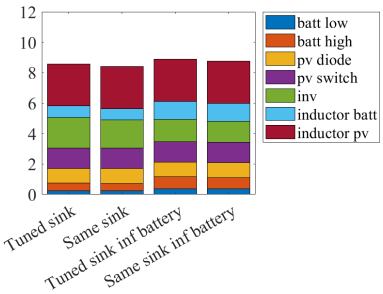

(a) DC-coupled converter

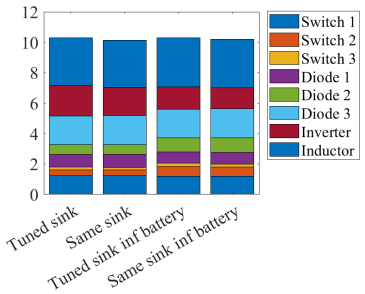

(b) MIMO converter

Fig. 8: Power loss [W] for optimised and identical heat sinks with either the rated or an infinite battery.

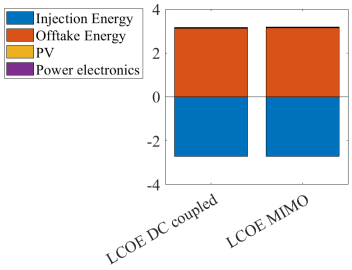

(a) Composition of the LCOE with both the contribution of energy injection and offtake.

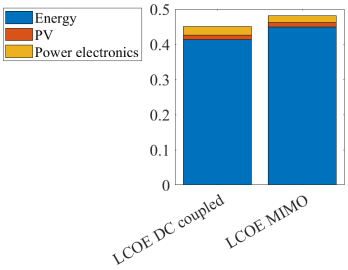

(b) Composition of the LCOE with net energy.

Fig. 9: LCOE [c/kWh] of the DC-coupled and MIMO converter with optimised heat sinks.

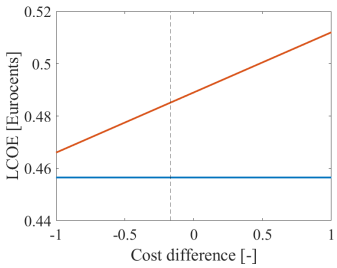

(a) Relative component cost difference.

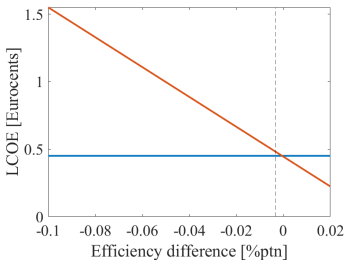

(b) Relative efficiency difference.

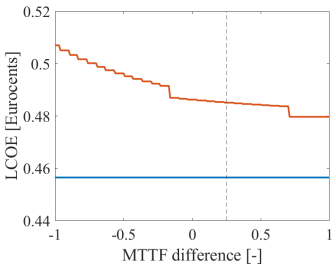

(c) Relative MTTF difference.

Fig. 10: Sensitivity analysis of the MIMO converter LCOE (red line), the DC-coupled converter values (blue line) are kept constant.

Table IV: Summary of the results from the LCOE analysis.

	Same sink		**Optimised sink**	
	DC-coupled	MIMO	DC-coupled	MIMO
Cinverter [-]	1	0.9542	1	0.8298
MTTF [-]	1.0030	2.0841	0.9981	1.2453
Efficiency [-]	0.9771	0.9738	0.9765	0.9734
LCOE [c/kWh]	0.4504	0.4778	0.4565	0.4851

Conclusion

This paper compared the LCOE of a DC-coupled and MIMO PV battery system in two different design cases. Next to the classical analysis taking into account the investment cost and fixed operational efficiency, this paper conducted a full electrothermal simulation of both systems. As result, a power flow dependent efficiency could be introduced together with mission profile dependent degradation. This influences the operation and maintenances expenses introducing new dependencies into the LCOE. The MIMO converter was shown to be more reliable and less expensive. However, the reduced efficiency of the MIMO converter due to the use of multiple diodes caused the resulting LCOE to be higher than the achieved results with the classical DC-coupled system. Future work will be devoted to improve the efficiency while keeping the reliability high and the manufacturing costs low. The sensitivity analysis showed that with only a slight improvement in efficiency, a big impact on the final LCOE can be made.

References

[1] S. Ravyts, M. D. Vecchia, G. V. den Broeck, and J. Driesen, "Review on building-integrated photovoltaics electrical system requirements and module-integrated converter recommendations," *Ener-*

gies, vol. 12, p. 1532, apr 2019.

[2] S. Danyali, S. H. Hosseini, and G. B. Gharehpetian, "New extendable single-stage multi-input dc-dc/ac boost converter," *IEEE Transactions on Power Electronics*, vol. 29, pp. 775–788, feb 2014.

[3] A. Pena-Bello, E. Barbour, M. Gonzalez, M. Patel, and D. Parra, "Optimized PV-coupled battery systems for combining applications: Impact of battery technology and geography," *Renewable and Sustainable Energy Reviews*, vol. 112, pp. 978–990, sep 2019.

[4] M. Sandelic, A. Sangwongwanich, and F. Blaabjerg, "Reliability evaluation of PV systems with integrated battery energy storage systems: DC-coupled and AC-coupled configurations," *Electronics*, vol. 8, p. 1059, sep 2019.

[5] L. Ayompe, A. Duffy, S. McCormack, and M. Conlon, "Projected costs of a grid-connected domestic pv system under different scenarios in ireland, using measured data from a trial installation," *Energy Policy*, vol. 38, pp. 3731–3743, jul 2010.

[6] F. L. Franco, A. Morandi, P. Raboni, and G. Grandi, "Efficiency comparison of dc and ac coupling solutions for large-scale pv bess power plants," *Energies*, vol. 14, p. 4823, aug 2021.

[7] Y. Khawaja, D. Giaouris, H. Patsios, and M. Dahidah, "Optimal cost-based model for sizing grid-connected PV and battery energy system," in *2017 IEEE Jordan Conference on Applied Electrical Engineering and Computing Technologies (AEECT)*, IEEE, oct 2017.

[8] W. Van De Sande, S. Ravyts, O. Alavi, P. Nivelle, J. Driesen, and M. Daenen, "The sensitivity of an electro-thermal photovoltaic dc–dc converter model to the temperature dependence of the electrical variables for reliability analyses," *Energies*, vol. 13, no. 11, 2020.

[9] W. V. D. Sande, S. Ravyts, A. Sangwongwanich, P. Manganiello, Y. Yang, F. Blaabjerg, J. Driesen, and M. Daenen, "A mission profile-based reliability analysis framework for photovoltaic DC-DC converters," *Microelectronics Reliability*, vol. 100-101, p. 113383, sep 2019.

[10] P. D. Reigosa, H. Wang, Y. Yang, and F. Blaabjerg, "Prediction of bond wire fatigue of igbts in a pv inverter under a long-term operation," *IEEE Transactions on Power Electronics*, vol. 31, no. 10, pp. 7171–7182, 2016.

[11] R. Bayerer, T. Herrmann, T. Licht, J. Lutz, and M. Feller, "Model for power cycling lifetime of igbt modules - various factors influencing lifetime," in *5th International Conference on Integrated Power Electronics Systems*, pp. 1–6, 2008.

[12] F. Hoffmann and N. Kaminski, "Power cycling capability and lifetime estimation of discrete silicon carbide power devices," *Materials Science Forum*, vol. 1004, p. 977, 07 2020.

[13] L. Ceccarelli, R. M. Kotecha, A. S. Bahman, F. Iannuzzo, and H. A. Mantooth, "Mission-profile-based lifetime prediction for a sic mosfet power module using a multi-step condition-mapping simulation strategy," *IEEE Transactions on Power Electronics*, vol. 34, no. 10, pp. 9698–9708, 2019.

[14] H. Wu, K. Sun, S. Ding, and Y. Xing, "Topology derivation of nonisolated three-port dc–dc converters from dic and doc," *IEEE Transactions on Power Electronics*, vol. 28, no. 7, pp. 3297–3307, 2013.

[15] T. Tjaden, J. Bergner, J. Weniger, and V. Quaschning, "Representative electrical load profiles of residential buildings in germany with a temporal resolution of one second," 12 2015.

[16] B. Zheng, J. Fletcher, A. Lennon, Y. Jiang, and P. Burr, "Solar irradiance measurements, with one second resolution, and estimated power ramp rate of photovoltaic modules with integrated capacitor energy storage. unsw, sydney.dataset.," 2019.